Mechanistic study of MUC3A in promoting progression of clear cell renal cell carcinoma via the JAK-STAT pathway

YONGYANG YUN[1-4*], XING JI[1-4*], SHUAI HU[1-4*], TIANYU WU[1-4], YIXIAO LIU[1-4], ZHENG LI[1-4], ZHOUJIE SUN[1-4], PEIMIN ZHOU[1-4], LEI YANG[1-4] and WEI YU[1-4]

[1]Department of Urology, Peking University First Hospital, Beijing 100034, P.R. China; [2]Institution of Urology, Peking University First Hospital, Peking University, Beijing 100034, P.R. China; [3]National Urological Cancer Center, Institute of Urology, Peking University First Hospital, Beijing 100034, P.R. China; [4]Beijing Key Laboratory of Urogenital Diseases (Male) Molecular Diagnosis and Treatment Center, Institute of Urology, Peking University First Hospital, Beijing 100034, P.R. China

Received July 25, 2025; Accepted March 11, 2026

DOI: 10.3892/or.2026.9119

Abstract. Clear cell renal cell carcinoma (ccRCC) is the most common subtype of renal cancer and is associated with poor prognosis. The present study identified a membrane-associated mucin, mucin 3A (MUC3A), a transmembrane glycoprotein, as a novel oncogenic factor in ccRCC. MUC3A was found to be highly expressed in ccRCC tissues and cell lines, with elevated levels associated with worse patient survival. Functional assays demonstrated that MUC3A knockdown significantly inhibited cell proliferation, migration, invasion, and promoted apoptosis. Mechanistically, MUC3A activated the Janus kinase-signal transducer and activator of transcription (JAK-STAT) signaling pathway, and activation of STAT3 reversed the effects of MUC3A knockdown. These findings suggest that MUC3A facilitates ccRCC progression via JAK/STAT signaling and may serve as a potential prognostic biomarker and therapeutic target.

Introduction

Renal cancer is the most prevalent malignancy affecting the urinary system, with both incidence and mortality rates rising steadily each year. In 2020, kidney cancer accounted for an estimated 431,288 new cases and 179,368 deaths worldwide, with ~73,600 new cases and ~25,200 deaths in China (1-3). Clear cell renal cell carcinoma (ccRCC) is the most common subtype, accounting for 70-80% of all renal cancer cases (4,5). Despite improvements in the diagnosis and treatment of ccRCC, the prognosis remains unfavorable, largely due to late-stage diagnosis, the tendency for metastasis and limited treatment options, particularly in advanced or refractory cases (6-8).

At the molecular level, ccRCC development and progression are driven by complex genetic, epigenetic and signaling alterations that collectively promote tumor growth, dissemination and therapeutic resistance. Among the pathways implicated in ccRCC biology, the Janus kinase-signal transducer and activator of transcription (JAK-STAT) signaling pathway has emerged as a critical regulator of renal tumorigenesis and disease aggressiveness (9,10). Activated primarily by cytokines and growth factors, the JAK-STAT pathway governs essential cellular processes, including proliferation, survival, differentiation and immune regulation (11). Accumulating evidence has indicated that the aberrant activation of JAK-STAT signaling, particularly persistent signal transducer and activator of transcription 3 (STAT3) activation, contributes to enhanced tumor cell growth, migration, resistance to apoptosis, and immune evasion in multiple malignancies, including ccRCC (12-19). In addition, dysregulated STAT3 signaling has been directly linked to ccRCC progression, drug resistance and aggressive clinical behavior (20-22).

Mucins are a family of high-molecular-weight glycoproteins that are predominantly expressed on epithelial surfaces, where they play essential roles in maintaining epithelial integrity, barrier function, and cell-cell communication. Beyond their physiological functions, aberrant mucin expression has been increasingly recognized as a contributor to tumor initiation, progression and metastasis (23,24). Among membrane-associated mucins, mucin 3A (MUC3A) is a transmembrane glycoprotein primarily localized to the apical surface of epithelial cells and has been implicated in regulating epithelial homeostasis and signaling processes (25,26).

Previous studies have identified MUC3A as an important oncogenic regulator in several malignancies. In colorectal cancer, MUC3A has been demonstrated to promote tumor progression through the activation of the PI3K/AKT/mTOR signaling pathway (27). In non-small cell lung cancer,

Correspondence to: Professor Wei Yu, Department of Urology, Peking University First Hospital, 8 Xishiku Street, Xicheng, Beijing 100034, P.R. China
Email: yuweif@126.com

*Contributed equally

Key words: clear cell renal cell carcinoma, membrane-associated mucins, mucin 3A, Janus kinase-signal transducer and activator of transcription signaling, signal transducer and activator of transcription 3, tumor progression, apoptosis, biomarker, targeted therapy

MUC3A was shown to contribute to tumor growth and radioresistance through the activation of NF-κB signaling and modulation of immune-related pathways, including programmed death-ligand 1 expression (28,29). In addition, emerging evidence suggests that MUC3A may participate in inflammatory and immune-related signaling networks, further supporting its potential role in shaping the tumor microenvironment (30,31).

Despite these findings in other cancer types, the expression pattern, biological function and mechanistic role of MUC3A in ccRCC remain largely unexplored. Given its membrane-associated structure, involvement in oncogenic signaling, and reported links to immune and inflammatory pathways, it is plausible that MUC3A may influence ccRCC progression through the modulation of key signaling cascades. In particular, the functional convergence between MUC3A-associated signaling and the JAK-STAT pathway raises the possibility that MUC3A may act as an upstream regulator or facilitator of JAK-STAT activation in ccRCC, a hypothesis that has not yet been systematically investigated.

The present study, sought to comprehensively characterize the expression and clinical relevance of MUC3A in ccRCC and explore its potential functional association with the JAK-STAT signaling pathway. By integrating bioinformatics analyses based on public datasets with *in vitro* functional and mechanistic experiments, the aim was to determine whether MUC3A contributes to ccRCC progression and to clarify its possible role in regulating JAK-STAT-mediated oncogenic processes. Through this approach, the present study provided novel insights into mucin-associated signaling in ccRCC and identified MUC3A as a potential molecular target worthy of further investigation.

Materials and methods

Cell culture. Human ccRCC cell lines 786-O (cat. no. CL-0010), OSRC-2 (cat. no. CL-0177), Caki-1 (cat. no. CL-0052) and ACHN (cat. no. CL-0021), as well as non-malignant renal epithelial cells HK-2 (cat. no. CL-0109; all from Procell Life Science & Technology Co., Ltd.) and RPTEC/TERT1 (cat. no. CRL-4031; American Type Culture Collection), were used in the present study. All cell lines were maintained in DMEM (Gibco; Thermo Fisher Scientific, Inc.) supplemented with 10% FBS (Gibco; Thermo Fisher Scientific, Inc.) and 1% penicillin-streptomycin, at 37˚C in a humidified incubator containing 5% CO_2.

Cells were routinely passaged every 2-3 days and used for experiments during the logarithmic growth phase. To minimize variability, all *in vitro* experiments were performed under identical culture conditions, and comparative analyses were conducted within the same cell line, with the control and treatment groups processed in parallel.

Small interfering RNA (siRNA) transfection. siRNAs targeting human MUC3A and a non-targeting negative control siRNA were synthesized by Shanghai GenePharma Co., Ltd., consistent with previously reported renal cell carcinoma studies (32,33). The siRNA sequences (RNA, U-bases) were as follows: Human mucin 3A (hMUC3A) si-1 sense, 5'-ACgACCUUCCCAgCAACAUAU-3' and antisense, 5'-AUAUgUUgCUgggAAggUCgU-3'; hMUC3A si-2 sense, 5'-CUACgUUgggUACCAUggUAA-3' and antisense, 5'-UUA CCAUggUACCCAACgUAg-3'; hMUC3A si-3 sense, 5'-ggA CCAACUUUCACAAgUA-3' and antisense, 5'-UACUUgUgA AAgUUggUCC-3'. The non-targeting negative control siRNA sequences (RNA, U-bases) were: Sense, 5'-UUCUCCGAA CGUGUCACGUdUdU-3' and antisense, 5'-ACGUGACAC GUUCGGAGAAdUdU-3'.

For functional assays, 786-O and OSRC-2 cells were seeded into 6-well plates at $2.5x10^5$ cells/well 24 h prior to transfection to reach 50-60% confluence at the time of transfection. siRNAs were transfected at a final concentration of 50 nM using Lipofectamine™ RNAiMAX (cat. no. 13778150; Thermo Fisher Scientific, Inc.) and Opti-MEM (Gibco; Thermo Fisher Scientific, Inc.), according to the manufacturer's isntructions. Briefly, siRNA and RNAiMAX (5 μl/well) were separately diluted in Opti-MEM, combined and incubated for 10-20 min at room temperature, and then added dropwise to the cells. A non-targeting siRNA (si-Ctrl) was used as the transfection control in all experiments.

After 6 h, the transfection medium was replaced with complete growth medium. Knockdown efficiency was evaluated by western blotting at 48 h post-transfection (relative to si-Ctrl). Unless otherwise indicated, CCK-8 proliferation and wound-healing assays were initiated at 24-48 h post-transfection; apoptosis analysis by flow cytometry and apoptosis-related western blotting were performed at 48 h post-transfection, and colony formation assays were initiated at 24 h post-transfection and maintained for 10-14 days. All experiments were performed with at least three independent biological replicates.

Western blotting. Total cellular proteins were extracted using RIPA lysis buffer supplemented with protease and phosphatase inhibitors (Beyotime Insitute of Biotechnology) on ice. Lysates were clarified by centrifugation at 12,000 x g for 15 min at 4˚C, and the supernatants were collected. Protein concentrations were determined using a BCA protein assay kit (Thermo Fisher Scientific, Inc.). Equal amounts of protein (30 μg per lane) were mixed with loading buffer, denatured at 95˚C for 5 min, separated by 8-12% SDS-PAGE and transferred onto polyvinylidene difluoride membranes (MilliporeSigma) using a wet transfer system at 300 mA for 90 min.

Membranes were blocked with 5% non-fat milk (Beijing Solarbio Science & Technology) in Tris-buffered saline with 0.1% Tween-20 (TBST) for 1 h at room temperature and incubated overnight at 4˚C with primary antibodies against MUC3A (rabbit polyclonal; cat. no. ab270247; dilution, 1:1,000; Abcam), JAK1 (rabbit monoclonal; cat. no. 3344; dilution, 1:1,000), phosphorylated (p)-JAK1 (Tyr1034/1035; rabbit monoclonal; cat. no. 74129; dilution, 1:1,000), STAT3 (rabbit monoclonal; cat. no. 9139; dilution, 1:1,000), p-STAT3 (Tyr705) (rabbit monoclonal; cat. no. #9145; dilution, 1:1,000), Bcl-2 (rabbit monoclonal; cat. no. #4223; dilution, 1:1,000), and cleaved Caspase-3 (rabbit monoclonal; cat. no. #9664; dilution, 1:1,000; all from Cell Signaling Technology, Inc.), and GAPDH (mouse monoclonal; cat. no. 60004-1-Ig; dilution, 1:5,000; Proteintech Group, Inc.). Membranes were washed in TBST (3 washes for 5-10 min) and incubated with HRP-conjugated secondary antibodies (anti-rabbit IgG; cat. no. 7074; dilution,

1:5,000; anti-mouse IgG; cat. no. 7076; dilution, 1:5,000; Cell Signaling Technology, Inc.) for 1 h at room temperature.

Protein bands were visualized using enhanced chemiluminescence reagents (Pierce™ ECL Western Blotting Substrate; cat. no. 32106; Thermo Fisher Scientific, Inc.) and quantified by ImageJ software (version 1.53; National Institutes of Health) (34,35). Densitometric values were normalized to GAPDH and expressed relative to the corresponding control group. All western blotting experiments were performed with at least three independent biological replicates.

Cell migration and invasion assays. Cell migration and invasion were assessed using Transwell chambers with 8-μm pore size polycarbonate membranes (cat. no. 3422, 12-well format; Corning, Inc.), as previously described in ccRCC studies (36,37). For migration assays, $5x10^4$ 786-O and OSRC-2 cells suspended in 100 μl serum-free medium were seeded into the upper chambers, while the lower chambers were filled with 800 μl complete medium containing 10% FBS as a chemoattractant.

For invasion assays, the upper chambers were pre-coated with Matrigel Basement Membrane Matrix (cat. no. 356234; Corning, Inc.), diluted at 1:8 in serum-free medium, and allowed to polymerize at 37˚C for 30 min prior to cell seeding. A total of $1x10^5$ 786-O and OSRC-2 cells in 100 μl serum-free medium were seeded per insert, and 800 μl complete medium with 10% FBS was added to the lower chamber. Cells were incubated at 37˚C for 24 h (migration) or 36-48 h (invasion). To minimize the influence of cell proliferation, cells were maintained under serum-free conditions in the upper chamber, and incubation times were kept within commonly used ranges.

Following incubation, non-migrated/non-invasive cells on the upper surface were gently removed using a cotton swab. Cells on the lower surface were fixed with 4% paraformaldehyde (Beijing Solarbio Science & Technology) for 15 min at room temperature, stained with 0.1% crystal violet (Beijing Solarbio Science & Technology) for 15 min at room temperature, and counted in five randomly selected, non-overlapping fields per insert under a light microscope (scale bar, 100 μm). Each condition was assayed in triplicate inserts and repeated in at least three independent biological experiments.

Wound healing assay. Cell migration was assessed using a wound healing assay. 786-O and OSRC-2 cells were seeded into 6-well plates and cultured until reaching near confluence (90-100%). A uniform scratch was generated across the cell monolayer using a sterile 200-μl pipette tip. Detached cells were gently removed by washing with PBS three times, and cells were subsequently cultured in serum-free DMEM to minimize the confounding effects of cell proliferation.

Images of the wound area were captured at 0 and 24 h under a light microscope at the same marked locations per well. Wound closure was quantified using ImageJ software (version 1.53) by measuring the wound area at each time point. The percentage of wound closure was calculated as $(A_o - A_t)/A_o \times 100\%$, where A_o is the wound area at 0 h and A_t is the wound area at 24 h (38). Each condition was assayed in triplicate wells and repeated in at least three independent biological experiments.

Cell proliferation assay. Cell proliferation was assessed using the Cell Counting Kit-8 (CCK-8; Dojindo Molecular Technologies, Inc.). 786-O and OSRC-2 cells were seeded into 96-well plates at a density of $5x10^2$ cells/well in 100 μl complete medium and allowed to attach overnight. Cells were then subjected to the indicated transfections/treatments. At 24, 48, 72 and 96 h, 10 μl CCK-8 reagent was added to each well and incubated for 2 h at 37˚C. Absorbance was measured at 450 nm using a microplate reader. Wells containing medium plus CCK-8 but without cells were used as blanks for background subtraction. The proliferation rate was determined based on the optical density readings following blank correction. Each condition was assayed in six replicate wells and repeated in at least three independent biological experiments.

Colony formation assay. To evaluate clonogenic ability, 786-O and OSRC-2 cells were seeded into 6-well plates at a density of 500 cells/well. Cells were subsequently transfected with si-MUC3A or the si-Ctrl as described above. Following transfection, cells were maintained in complete medium, which was refreshed every 2 days, and colonies were allowed to form for 10-14 days.

At the end of the incubation period, colonies were fixed with 4% paraformaldehyde for 15 min at room temperature and stained with 0.1% crystal violet dye for 15 min at room temperature. Colonies containing >50 cells were counted manually under a light microscope (Leica DMi1; Leica Microsystems GmbH). Clonogenic efficiency was quantified as the number of colonies per well. Each condition was assayed in triplicate wells and repeated in at least three independent biological experiments.

Flow cytometric analysis of apoptosis. Apoptosis was assessed by flow cytometry using Annexin V-FITC/propidium iodide (PI) staining. 786-O and OSRC-2 cells were harvested 48 h following transfection, washed twice with cold PBS, and resuspended in 1X binding buffer. For each sample, $1x10^5$ cells were stained according to the manufacturer's instructions using an Annexin V-FITC Apoptosis Detection Kit (cat. no. 556547; BD Biosciences). Briefly, cells were incubated with Annexin V-FITC and PI for 15 min at room temperature in the dark, followed by the addition of binding buffer prior to acquisition.

Flow cytometric analysis was performed on a BD FACSCanto II flow cytometer (BD Biosciences). Unstained cells, single-stained controls and negative controls were included for compensation and gating. A minimum of 10,000 events per sample was collected. Initial gating was performed on forward scatter versus side scatter to exclude debris, followed by quadrant analysis of Annexin V-FITC and PI to distinguish viable (Annexin V^-/PI^-), early apoptotic (Annexin V^+/PI^-) and late apoptotic/necrotic (Annexin V^+/PI^+) cells. Total apoptosis was calculated as the sum of early and late apoptotic populations (Annexin V^+/PI^- + Annexin V^+/PI^+). Data were analyzed using FlowJo software (version 11; BD Biosciences) (39,40). Each condition was assayed in triplicate and repeated in at least three independent biological experiments.

In silico analysis. Publicly available transcriptomic data and corresponding clinical information of patients with ccRCC were obtained from The Cancer Genome Atlas (TCGA)

database through the Genomic Data Commons data portal (https://portal.gdc.cancer.gov/). RNA sequencing data [HTSeq-transcripts per million (TPM) format] from the TCGA-kidney renal clear cell carcinoma (KIRC) cohort were downloaded and used for subsequent analyses. Pan-cancer expression analysis of MUC3A was performed using the Gene Expression Profiling Interactive Analysis 2 (GEPIA2) web server (http://gepia2.cancer-pku.cn/). MUC3A expression levels across different tumor types were visualized using the 'Expression Analysis - General' module with log2(TPM + 1) normalization. Differential expression of MUC3A between tumor and normal tissues in the TCGA-KIRC cohort was evaluated using the 'Expression DIY - Boxplot' module, with the following parameters: |log2 fold change| cutoff=1 and P-value cutoff=0.01, using matched TCGA normal samples when available.

Survival analysis was conducted using GEPIA2 based on TCGA-KIRC data. Overall survival (OS) and disease-free survival (DFS) were analyzed by stratifying patients into high- and low-expression groups according to MUC3A expression levels. For OS analysis, the expression cutoff was set at the upper 80% vs. lower 20%, while for DFS analysis, the cutoff was set at 87.5% vs. 12.5%. Kaplan-Meier survival curves were generated, and statistical significance was assessed using the log-rank test.

For pathway enrichment analyses, differentially expressed genes associated with MUC3A expression were identified, and genes with $P<0.05$ were selected for downstream functional analysis. Kyoto Encyclopedia of Genes and Genomes (KEGG) pathway enrichment analysis was performed using the clusterProfiler R package (version 4.12.6; Bioconductor; https://bioconductor.org/packages/release/bioc/html/clusterProfiler.html) with the enrichKEGG function. Gene set enrichment analysis (GSEA) was conducted using the GSEA function implemented in the same package to assess pathway-level differences between high- and low-MUC3A expression groups. Enrichment results were visualized using standard plotting functions provided by the clusterProfiler package.

Statistical analysis. All experiments were performed with at least three independent biological replicates ($n\geq3$), and data are presented as the mean ± standard deviation (SD) unless otherwise stated. Statistical analyses were conducted using GraphPad Prism 9 (GraphPad Software, Inc.; Dotmatics). For comparisons between two groups, a two-tailed unpaired Student's t-test was used. For comparisons among multiple groups, one- or two-way analysis of variance (ANOVA) was performed as appropriate, followed by Dunnett's post hoc test (when comparing multiple groups to a single control) or Tukey's post hoc test (for all pairwise comparisons), as indicated in the figure legends. Fold-change values were calculated relative to the corresponding control group where applicable. $P<0.05$ was considered to indicate a statistically significant difference. Significance levels are denoted as $P<0.05$, $P<0.01$ and $P<0.001$, unless otherwise specified.

Results

High expression of MUC3A in ccRCC is associated with poor prognosis. First, as shown in Fig. 1A, a pan-cancer analysis of MUC3A expression was performed and it was found that MUC3A was significantly upregulated in multiple tumor types, including colon adenocarcinoma (COAD), cholangiocarcinoma (CHOL), and KIRC. Furthermore, in unpaired samples from the TCGA-KIRC cohort (523 tumor samples vs. 72 normal samples), MUC3A expression levels were markedly higher in tumor tissues than adjacent normal tissues (Fig. 1B). To confirm the oncogenic role of MUC3A in ccRCC, MUC3A expression was assessed in HK-2 and RPTEC/TERT1 non-malignant renal epithelial cell lines, as well as in CAKI-1, OSRC-2, 786-O and ACHN renal cancer cell lines. The findings showed elevated protein levels of MUC3A in renal cancer cell lines compared with non-malignant renal epithelial cell lines (Fig. 1C). Data from the TCGA database revealed that patients with high MUC3A expression exhibited a significantly poorer OS and DFS than patients with low MUC3A expression (Fig. 1E and F). These findings indicated that MUC3A is aberrantly upregulated in ccRCC and that elevated MUC3A expression is associated with unfavorable clinical outcomes.

Knockdown of MUC3A suppresses ccRCC cell proliferation and colony-forming ability. To investigate the functional role of MUC3A in ccRCC, siRNA targeting MUC3A was used to transiently knock down MUC3A in two cell lines with the highest endogenous expression (786-O and OSRC-2), and knockdown efficiency was verified. Among the tested siRNAs, si-2 exhibited the most effective silencing (Fig. 1D). si-2 was selected for subsequent functional experiments due to its superior knockdown efficiency.

In the CCK-8 assay, MUC3A knockdown resulted in a modest but statistically significant reduction in cell proliferation in 786-O cells (~10% decrease compared with siCtrl; $P<0.01$), whereas a more pronounced inhibitory effect was observed in OSRC-2 cells, with proliferation reduced by more than threefold ($P<0.001$; Fig. 2A and B). Consistently, the colony formation assay showed that MUC3A knockdown significantly impaired clonogenic ability, with the number of colonies reduced by ~30% in 786-O cells and 40% in OSRC-2 cells (both $P<0.05$), as compared with control groups (Fig. 2C and D).

MUC3A knockdown promotes apoptosis in ccRCC cells. To elucidate the effect of MUC3A on apoptosis, Annexin V-FITC/PI staining was performed followed by flow cytometric analysis. It was observed that MUC3A knockdown led to a significant increase in apoptotic cell populations in both 786-O and OSRC-2 cells (Fig. 2E and F). Quantitative analysis showed that the apoptotic rate in OSRC-2 cells increased to approximately threefold that of the control group, while a roughly two-fold increase was observed in 786-O cells following MUC3A silencing (both $P<0.001$).

MUC3A knockdown inhibits ccRCC cell migration and invasion. Transwell migration and Transwell invasion assays, as well as wound healing assays, were performed to investigate the role of MUC3A in ccRCC cell motility. Transwell migration assays demonstrated a marked suppression of migratory capacity following MUC3A silencing. Quantitative analysis showed that the migratory rate of 786-O cells was reduced to ~50% of control levels ($P<0.01$), whereas a more pronounced

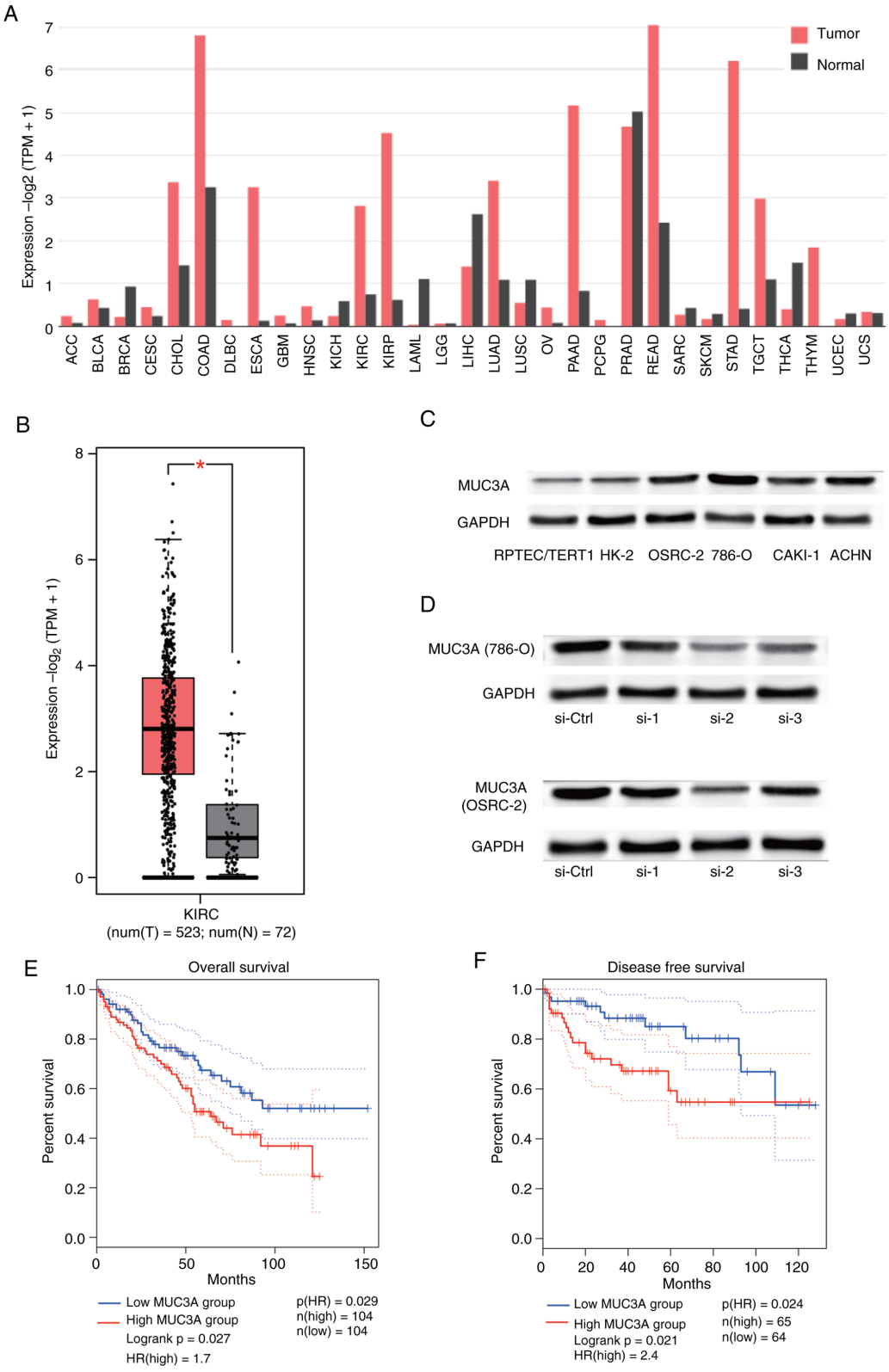

Figure 1. MUC3A is aberrantly upregulated in ccRCC and associated with poor prognosis. (A) Pan-cancer analysis of MUC3A expression across multiple tumor types based on TCGA data, generated using the GEPIA2 platform. Gene expression values are presented as log2(TPM + 1). (B) Differential expression of MUC3A in tumor and normal samples from the TCGA-KIRC cohort (523 tumor samples vs. 72 normal samples). *P<0.05. (C) Western blotting of MUC3A protein expression in HK-2 and RPTEC/TERT1 non-malignant renal epithelial cell lines and ccRCC cell lines (CAKI-1, OSRC-2, 786-O and ACHN). GAPDH was used as a loading control. (D) Western blotting of MUC3A knockdown efficiency in 786-O and OSRC-2 cells following transient transfection with three independent siRNAs targeting MUC3A. si-2 was selected for subsequent functional experiments due to its superior knockdown efficiency. (E) Kaplan-Meier OS analysis of ccRCC patients stratified into high- and low-MUC3A expression groups using the GEPIA2 platform. (F) Kaplan-Meier DFS analysis of ccRCC patients based on MUC3A expression levels. Data are derived from TCGA unless otherwise indicated. MUC3A, mucin 3A; ccRCC, clear cell renal cell carcinoma; TCGA, The Cancer Genome Atlas; KIRC, kidney renal clear cell carcinoma; GEPIA2, Gene Expression Profiling Interactive Analysis 2; TPM, transcripts per million; KIRC, kidney renal clear cell carcinoma; OS, overall survival; DFS, disease-free survival; siRNA, small interfering RNA; si-MUC3A, MUC3A-targeting siRNA; si-Ctrl, non-targeting control siRNA; GAPDH, glyceraldehyde-3-phosphate dehydrogenase; si-1/si-2/si-3, three independent siRNAs targeting MUC3A.

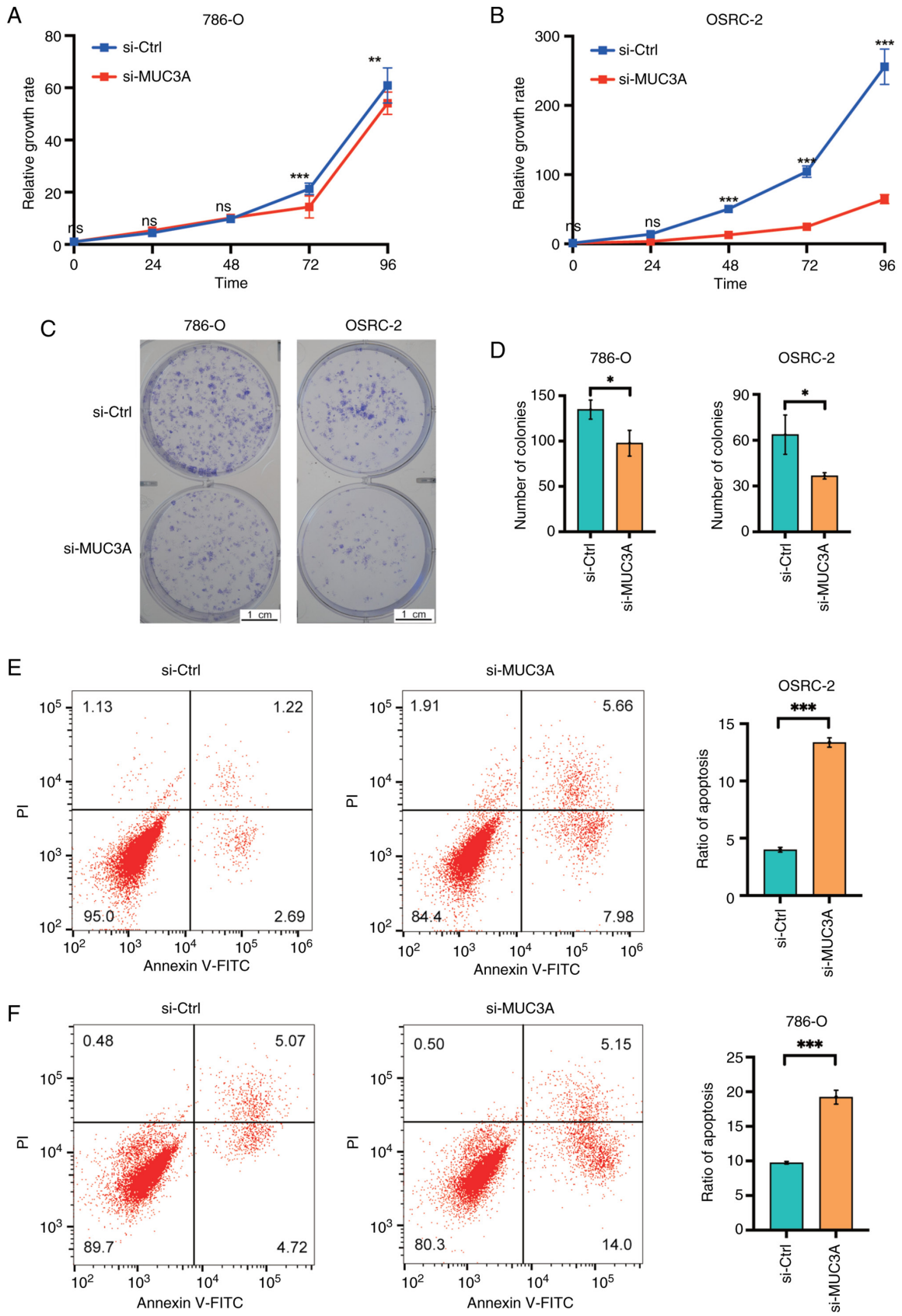

Figure 2. MUC3A knockdown suppresses proliferation and promotes apoptosis in ccRCC cells. (A and B) Cell proliferation of 786-O and OSRC-2 cells following transfection with si-MUC3A or si-Ctrl, as assessed by CCK-8 assays at the indicated time points. (C and D) Colony formation assays showing the clonogenic capacity of 786-O and OSRC-2 cells following MUC3A knockdown. Representative images and quantitative analysis are shown. (E and F) Flow cytometric analysis of apoptosis in 786-O and OSRC-2 cells using Annexin V-FITC/PI staining following MUC3A silencing. Representative dot plots and corresponding quantitative results are presented. All experiments were performed with at least three independent biological replicates (n≥3). Data are presented as the mean ± SD. Statistical significance was determined using a two-tailed unpaired Student's t-test. *P<0.05, **P<0.01 and ***P<0.001. MUC3A, mucin 3A; ccRCC, clear cell renal cell carcinoma; CCK-8, Cell Counting Kit-8; si-MUC3A, MUC3A-targeting siRNA; si-Ctrl, non-targeting control siRNA; PI, propidium iodide; SD, standard deviation; ns, not significant.

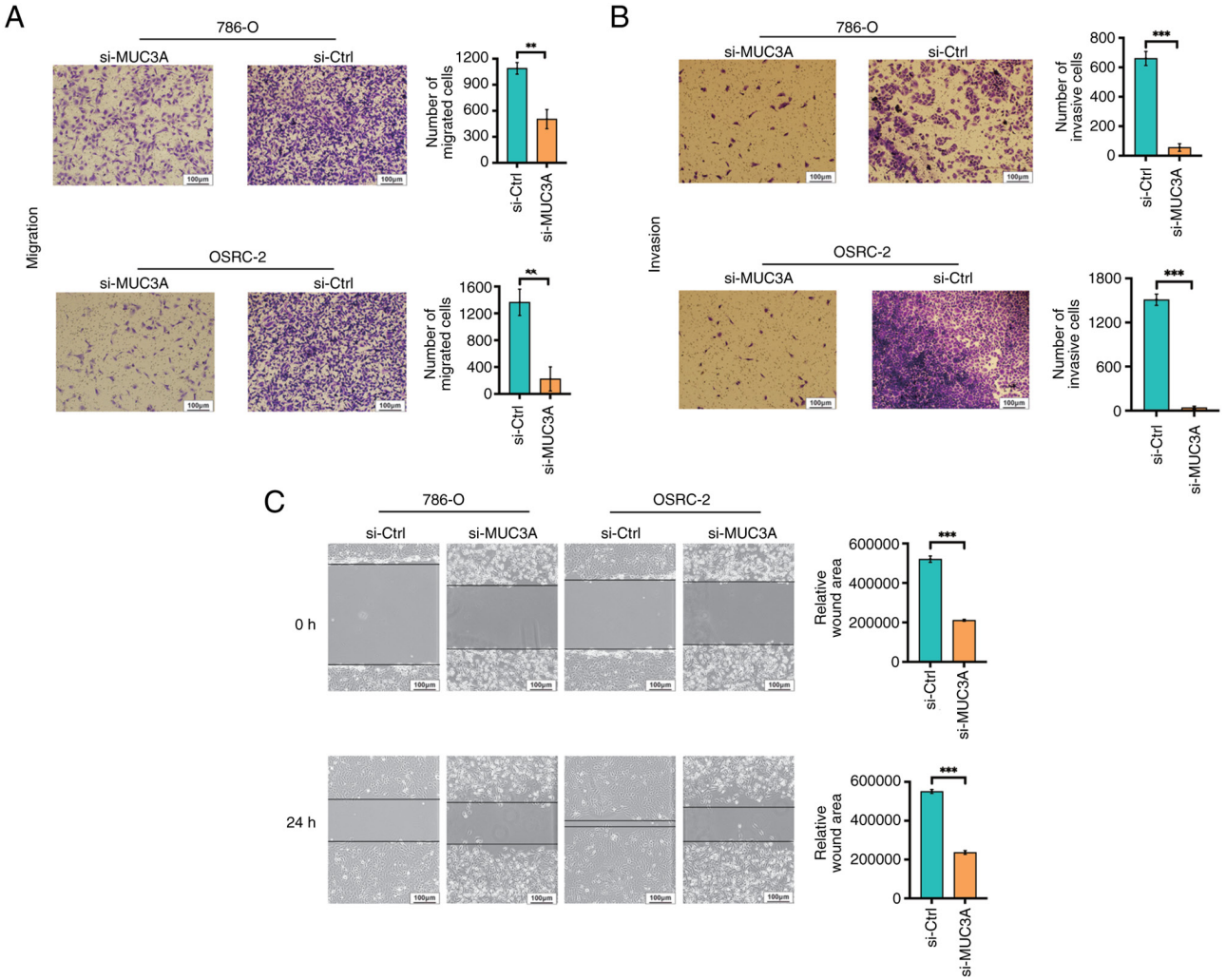

Figure 3. MUC3A knockdown inhibits the migration and invasion of ccRCC cells. (A) Transwell migration assays showing the migratory capacity of 786-O and OSRC-2 cells following MUC3A knockdown. Quantitative analysis is shown on the right. (B) Transwell invasion assays performed using Matrigel®-coated chambers to assess the invasive potential of ccRCC cells after MUC3A silencing. (C) Wound healing assays demonstrating delayed wound closure in 786-O and OSRC-2 cells transfected with si-MUC3A compared with si-Ctrl at 24 h. Representative images and quantitative analyses are shown. Scale bar, 100 μm. All experiments were conducted with at least three independent biological replicates. Data are expressed as the mean ± SD. **P<0.01 and ***P<0.001. MUC3A, mucin 3A; ccRCC, clear cell renal cell carcinoma; si-MUC3A, MUC3A-targeting siRNA; si-Ctrl, non-targeting control siRNA; SD, standard deviation.

inhibitory effect was observed in OSRC-2 cells, with migration reduced to ~1/7 of the control levels (P<0.01; Fig. 3A).

Furthermore, Transwell invasion assays revealed a marked inhibitory effect of MUC3A knockdown on invasive capacity (Fig. 3B). Compared with control cells, the number of invasive 786-O cells was reduced by more than one order of magnitude, whereas OSRC-2 cells exhibited an even more pronounced reduction, approaching two orders of magnitude, following MUC3A silencing. Collectively, these results indicated that MUC3A plays an important role in promoting the migratory and invasive phenotypes of ccRCC cells.

Consistently, in the wound healing assay, MUC3A knockdown significantly delayed wound closure in both 786-O and OSRC-2 cells, with the migration rate reduced by ~50% compared with control cells (P<0.001; Fig. 3C).

MUC3A knockdown downregulates the JAK-STAT signaling pathway in ccRCC. To further explore the potential mechanisms through which MUC3A contributes to ccRCC progression, KEGG pathway enrichment analysis was performed based on MUC3A expression levels. The results indicated that MUC3A expression was associated with multiple signaling pathways, including 'primary immunodeficiency', 'oxidative phosphorylation', 'Th17 cell differentiation', 'NF-κB signaling' and 'cytokine-cytokine receptor interaction' (Fig. 4A).

Of note, GSEA revealed a significant enrichment of the JAK-STAT signaling pathway in samples with high MUC3A expression (Fig. 4B). Given the established role of the JAK-STAT pathway in regulating key biological processes such as cell proliferation, apoptosis and immune responses, these findings suggested a potential link between MUC3A and JAK-STAT pathway activation in ccRCC.

To further validate this association at the protein level, western blotting was performed, which demonstrated that MUC3A knockdown resulted in reduced phosphorylation levels of JAK1, JAK2 and STAT3, while total protein levels remained largely unchanged (Fig. 4C and D). To further validate the involvement of the JAK-STAT pathway, 786-O and OSRC-2 cells were treated with Colivelin trifluoroacetate

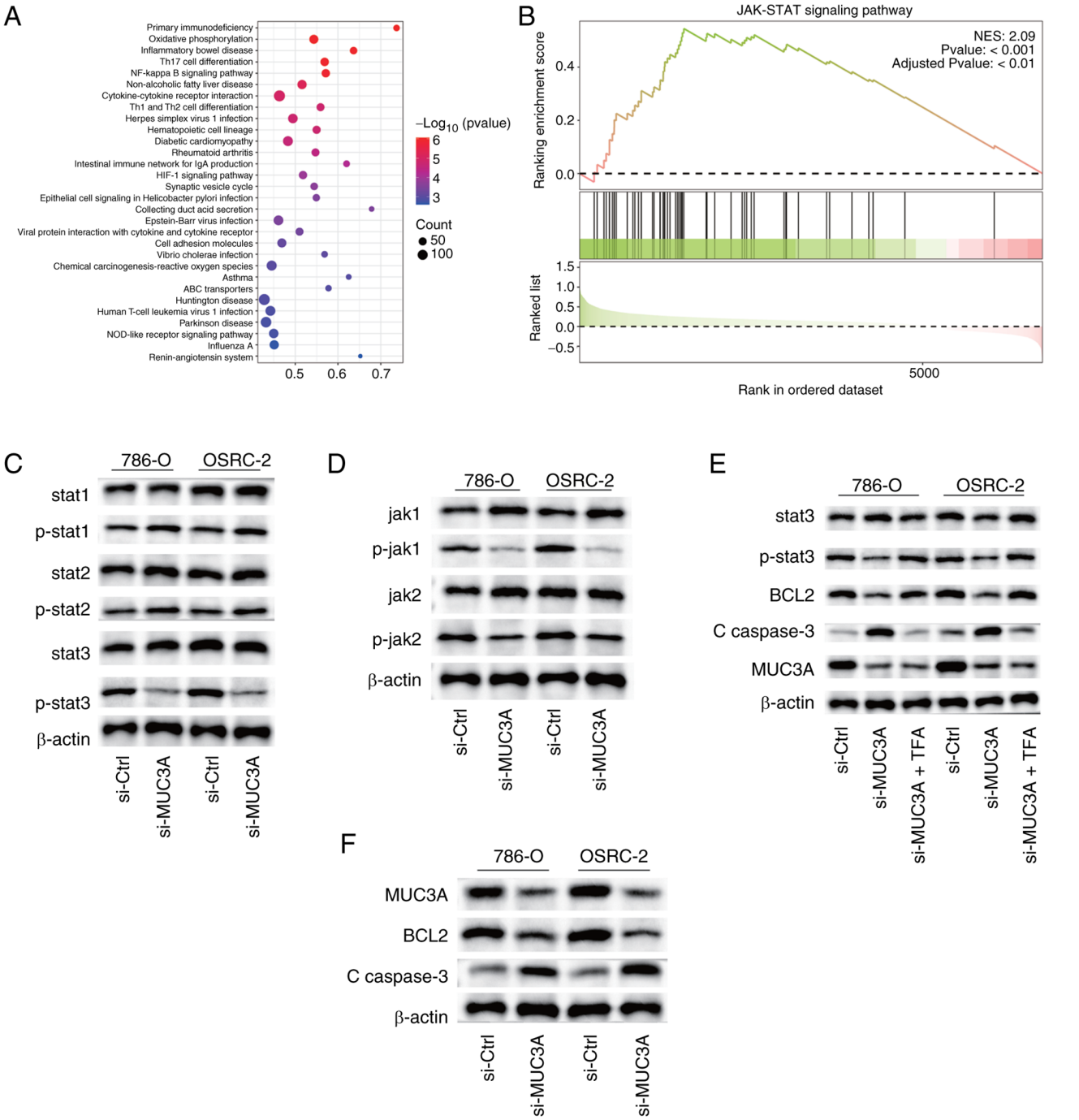

Figure 4. MUC3A is associated with the activation of the JAK-STAT signaling pathway in ccRCC. (A) KEGG pathway enrichment analysis of genes associated with MUC3A expression based on TCGA-KIRC transcriptomic data. (B) GSEA showing significant enrichment of the JAK-STAT signaling pathway in ccRCC samples with a high MUC3A expression. (C and D) Western blotting of total and phosphorylated JAK1, JAK2 and STAT3 in 786-O and OSRC-2 cells following MUC3A knockdown. (E) Western blotting showing that STAT3 activation by Colivelin TFA restores p-STAT3 levels in si-MUC3A-transfected 786-O and OSRC-2 cells, accompanied by increased Bcl-2 and decreased cleaved caspase-3 expression. (F) Western blotting of apoptosis-related proteins Bcl-2 and cleaved caspase-3 following MUC3A silencing. GAPDH served as a loading control. All western blotting experiments were repeated independently at least three times. MUC3A, mucin 3A; JAK, Janus kinase; STAT, signal transducer and activator of transcription; ccRCC, clear cell renal cell carcinoma; KEGG, Kyoto Encyclopedia of Genes and Genomes; TCGA, The Cancer Genome Atlas; KIRC, kidney renal clear cell carcinoma; GSEA, gene set enrichment analysis; TFA, trifluoroacetate; p-, phosphorylated.

(TFA), a specific STAT3 agonist, following MUC3A knockdown. At the protein level, p-STAT3 expression was restored in the si-MUC3A + Colivelin TFA group, accompanied by increased Bcl-2 and decreased cleaved caspase-3 levels (Fig. 4E). Furthermore, consistent with the flow cytometric findings aforementioned, western blotting demonstrated a marked decrease in the expression of the anti-apoptotic protein Bcl-2, accompanied by increased levels of cleaved caspase-3 upon MUC3A knockdown (Fig. 4F). Collectively, these results supported the notion that MUC3A may promote ccRCC progression, at least in part, through modulation of the JAK-STAT signaling pathway.

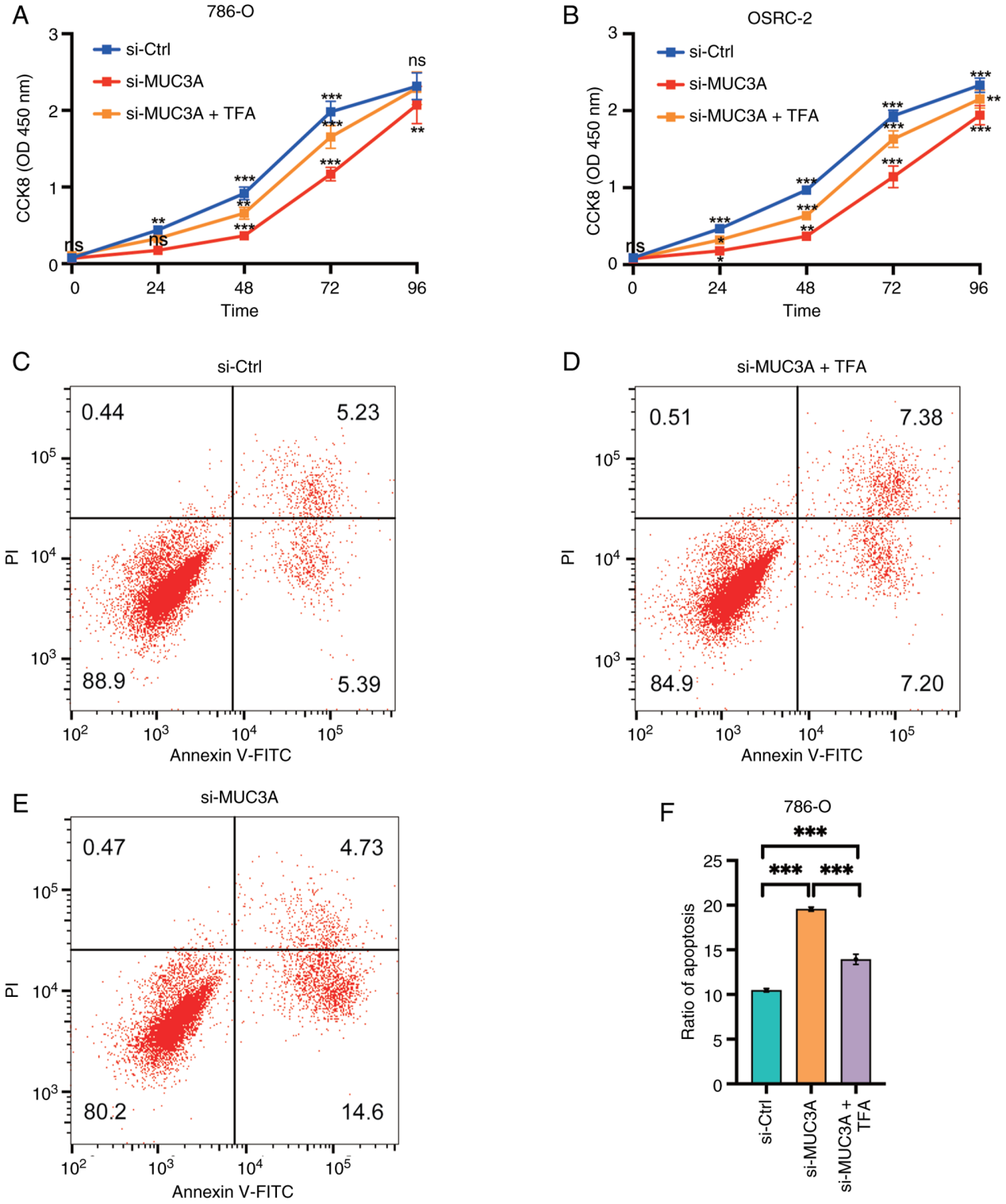

Figure 5. STAT3 activation partially rescues the effects of MUC3A knockdown in ccRCC cells. (A and B) CCK-8 assays showing that treatment with the STAT3 agonist Colivelin TFA partially restored the proliferation of 786-O and OSRC-2 cells following MUC3A knockdown. (C-F) Flow cytometric analysis demonstrating that Colivelin TFA treatment reverses the apoptosis-promoting effect induced by MUC3A silencing in ccRCC cells. Data are presented as the mean ± SD from at least three independent biological replicates. Statistical significance was assessed using Student's t-test or one-way ANOVA as appropriate. *P<0.05, **P<0.01 and ***P<0.001. STAT3, signal transducer and activator of transcription 3; TFA, trifluoroacetate; MUC3A, mucin 3A; CCK-8, Cell Counting Kit-8; si-MUC3A, MUC3A-targeting siRNA; si-Ctrl, non-targeting control siRNA; SD, standard deviation; ANOVA, analysis of variance.

MUC3A regulates ccRCC proliferation and apoptosis via the JAK-STAT pathway. Building on the protein-level validation of JAK-STAT activation, the functional consequences of restoring this pathway were next examined. Treatment with Colivelin TFA rescued the proliferation inhibition caused by si-MUC3A, restoring cell growth to levels comparable to those of the controls (Fig. 5A and B). Similarly, the apoptosis-promoting effect of MUC3A knockdown was reversed upon Colivelin TFA treatment (Fig. 5C-F). These findings indicated that MUC3A promotes ccRCC proliferation and

suppresses apoptosis through the activation of the JAK-STAT signaling pathway.

Discussion

In the present study, the expression, functional relevance and potential signaling mechanisms of MUC3A were systematically investigated in ccRCC. The findings demonstrated that MUC3A is aberrantly upregulated in ccRCC and that its silencing leads to a significant suppression of tumor-associated phenotypes, including cell proliferation, clonogenic capacity, migration, invasion and resistance to apoptosis. Collectively, these results supported the role for MUC3A as a contributor to ccRCC progression rather than a passive bystander.

Mucins have long been recognized as important regulators of epithelial biology, and accumulating evidence suggests that dysregulated mucin expression contributes to tumorigenesis through mechanisms involving cell adhesion, immune evasion and intracellular signaling modulation. Previous studies on mucins, such as MUC1 and MUC4, have established their oncogenic roles in multiple malignancies, including colorectal, pancreatic and lung cancer, where they participate in signal transduction and promote aggressive tumor behavior (23,24). These findings extend this concept by identifying MUC3A as a functionally relevant mucin in ccRCC, a cancer type in which the role of membrane-related mucins has been comparatively underexplored.

A key observation of the present study is the association between MUC3A expression and activation of the JAK-STAT signaling pathway in ccRCC. Through integrated bioinformatics analyses and experimental validation, it was found that MUC3A knockdown resulted in the reduced phosphorylation of JAK1, JAK2 and STAT3, without substantially affecting total protein levels. These findings suggested that MUC3A may influence ccRCC progression, at least in part, by modulating the activity of the JAK-STAT pathway rather than altering its basal expression. Of note, the present results do not imply that MUC3A is the sole upstream regulator of JAK-STAT signaling; instead, they indicate that MUC3A may function as a facilitator or enhancer within a broader oncogenic signaling network.

The biological relevance of JAK-STAT signaling in ccRCC has been well documented. Persistent activation of STAT3 has been shown to drive tumor cell proliferation, enhance migratory and invasive potential, promote resistance to apoptosis and contribute to immune evasion in renal cancer (20-22). The present data were consistent with these observations and further suggested that MUC3A may represent one of the upstream molecular factors capable of shaping STAT3 activation status in ccRCC cells. Of note, rescue experiments using a STAT3 agonist partially reversed the anti-proliferative and pro-apoptotic effects induced by MUC3A silencing, providing functional support for the involvement of JAK-STAT signaling downstream of MUC3A. Consistent with this mechanism-oriented interpretation, a recent ccRCC study reported that apolipoprotein C2 promotes malignant phenotypes at least partly through the activation of the JAK-STAT pathway, supporting the concept that distinct upstream molecules may converge on JAK/STAT signaling to drive ccRCC progression (41). In addition, a recent systematic review highlighted JAK/STAT as a major signaling axis in renal carcinoma and summarized its therapeutic potential, which further supported the translational relevance of the present findings linking MUC3A to JAK/STAT activation (42).

From a translational perspective, the JAK-STAT pathway has emerged as a promising therapeutic target in multiple malignancies, including renal cancer. Pharmacological inhibitors of the JAK or STAT signaling, such as ruxolitinib, are currently being evaluated in preclinical and clinical settings, either as monotherapies or in combination with other agents (9). In this context, the present findings raise the possibility that MUC3A expression status may help identify a subset of patients with ccRCC who are more likely to benefit from therapies targeting the JAK-STAT axis. In addition, therapeutic strategies aimed at reducing MUC3A expression or disrupting its functional interactions could potentially enhance the efficacy of JAK-STAT-directed treatments.

Despite the strengths of the present study, several limitations should be acknowledged. First, although TCGA-based analyses provide valuable insights into gene expression patterns and clinical associations at the tissue level, such data reflect bulk tumor samples and cannot fully capture intratumoral heterogeneity or microenvironmental influences. Secondly, these functional experiments were conducted in immortalized ccRCC cell lines cultured under standardized *in vitro* conditions. While all comparisons were performed under identical conditions, the use of DMEM rather than RPMI-1640 may influence cellular behavior and signaling responses, and this potential confounding factor cannot be completely excluded. Thirdly, the absence of *in vivo* validation limits the direct translational applicability of the present findings.

Future studies should focus on elucidating the precise molecular mechanisms through which MUC3A interfaces with JAK-STAT signaling, including whether this regulation occurs through direct protein interactions or via intermediary signaling molecules. In addition, given the central role of JAK-STAT signaling in immune regulation, it will be important to explore the contribution of MUC3A to immune modulation and immune checkpoint responsiveness in ccRCC. Finally, *in vivo* studies using xenograft or patient-derived xenograft models will be essential to validate the oncogenic role of MUC3A and to assess its potential as a therapeutic target in clinically relevant settings.

To the best of our knowledge, the present study is the first to systematically characterize the expression, functional significance and mechanistic role of MUC3A in ccRCC. While the JAK-STAT pathway has been extensively implicated in ccRCC, the involvement of MUC3A as a modulator of this signaling axis has not been previously reported. By integrating bioinformatics analyses with functional and rescue experiments, the present study identified MUC3A as a previously underappreciated contributor to ccRCC progression.

In conclusion, MUC3A was identified herein as a previously underappreciated contributor to ccRCC progression and provided evidence linking its oncogenic effects to the modulation of the JAK-STAT signaling pathway. These findings expanded the current understanding of mucin biology in renal cancer and highlighted MUC3A as a potential biomarker and therapeutic target worthy of further investigation.

In conclusion, the present study provided novel insights into the oncogenic role of MUC3A in ccRCC and highlighted its potential as a therapeutic target. By elucidating the mechanistic relationship between MUC3A and the JAK/STAT signaling pathway, the groundwork was laid for future studies aimed at developing targeted therapies that can improve the prognosis of ccRCC patients.

Acknowledgements

The authors would like to thank the staff of the Department of Urology, Peking University First Hospital (Beijing, China), for their technical support and insightful discussions.

Funding

The present study was supported by the Beijing Natural Science Foundation (grant no. 7232179).

Availability of data and materials

All data generated or analyzed during this study are included in this published article.

Authors' contributions

YY conceived and designed the study, performed the major experiments, analyzed and interpreted the data, and drafted the manuscript. XJ contributed to the study design, performed key experiments, and participated in data analysis and manuscript revision. SH contributed to experimental work and data collection, and participated in data analysis and manuscript revision. TW, YL, ZL, ZS, PZ and LY provided technical assistance and helped with data collection and/or verification. WY conceived and supervised the study, contributed to the study design and data interpretation, and critically revised the manuscript. YY and WY confirm the authenticity of all the raw data. All authors have read and approved the final manuscript.

Ethics approval and consent to participate

Not applicable.

Patient consent for publication

Not applicable.

Competing interests

The authors declare that they have no competing interests.

References

1. Yao L, Du Y, Dong W, Gao X, Guo J, Qiu J, Wei Q, Wu S, Ye D, Yu W, *et al*: Chinese quality control indices for standardized diagnosis and treatment of renal cancer (2022 edition). J Natl Cancer Cent 4: 6-13, 2024.
2. Sung H, Ferlay J, Siegel RL, Laversanne M, Soerjomataram I, Jemal A and Bray F. Global cancer statistics 2020: GLOBOCAN estimates of incidence and mortality worldwide for 36 cancers in 185 countries. CA Cancer J Clin 71: 209-249, 2021.
3. Capitanio U, Bensalah K, Bex A, Boorjian SA, Bray F, Coleman J, Gore JL, Sun M, Wood C and Russo P: Epidemiology of renal cell carcinoma. Eur Urol 75: 74-84, 2019.
4. Siegel RL, Miller KD, Fuchs HE and Jemal A: Cancer statistics, 2022. CA Cancer J Clin 72: 7-33, 2022.
5. Lv XQ, Zhang KB, Guo X, Pei L and Li F: Higher TYROBP and lower SOX6 as predictive biomarkers for poor prognosis of clear cell renal cell carcinoma: A pilot study. Medicine (Baltimore) 101: e30658, 2022.
6. Colombo PE, Quenet F, Alric P, Mourregot A, Neron M, Portales F, Rouanet P and Carrier G: Distal pancreatectomy with celiac axis resection (Modified Appleby Procedure) and arterial reconstruction for locally advanced pancreatic adenocarcinoma after FOLFIRINOX chemotherapy and chemoradiation therapy. Ann Surg Oncol 28: 1106-1108, 2021.
7. Zhang Q, Ren H, Ge L, Zhang W, Song F and Huang P: A review on the role of long non-coding RNA and microRNA network in clear cell renal cell carcinoma and its tumor microenvironment. Cancer Cell Int 23: 16, 2023.
8. Song Z, Guan C, Li T, Li C, Zhang N, Liu K, Yang C, Zhu Y and Xu Y: Vaporization phosphorization-mediated synthesis of phosphorus-doped TiO_2 nanocomposites for combined photodynamic and photothermal therapy of renal cell carcinoma. J Mater Chem B 12: 4039-4052, 2024.
9. Meng K, Li YY, Liu DY, Hu LL, Pan YL, Zhang CZ and He QY: A five-protein prognostic signature with GBP2 functioning in immune cell infiltration of clear cell renal cell carcinoma. Comput Struct Biotechnol J 21: 2621-2630, 2023.
10. Gao Y, Qi JC, Li X, Sun JP, Ji H and Li QH: Decreased expression of TXNIP predicts poor prognosis in patients with clear cell renal cell carcinoma. Oncol Lett 19: 763-770, 2020.
11. Sánchez A and Fabregat I: Growth factor- and cytokine-driven pathways governing liver stemness and differentiation. World J Gastroenterol 16: 5148-5161, 2010.
12. Sabaawy HE, Ryan BM, Khiabanian H and Pine SR: JAK/STAT of all trades: linking inflammation with cancer development, tumor progression and therapy resistance. Carcinogenesis 42: 1411-1419, 2021.
13. Owen KL, Brockwell NK and Parker BS: JAK-STAT signaling: A double-edged sword of immune regulation and cancer progression. Cancers (Basel) 11: 2002, 2019
14. Rah B, Rather RA, Bhat GR, Baba AB, Mushtaq I, Farooq M, Yousuf T, Dar SB, Parveen S, Hassan R, *et al*: JAK/STAT signaling: molecular targets, therapeutic opportunities, and limitations of targeted inhibitions in solid malignancies. Front Pharmacol 13: 821344, 2022.
15. Pang S, Zhao S, Dongye Y, Fan Y and Liu J: Identification and validation of m6A-associated ferroptosis genes in renal clear cell carcinoma. Cell Biol Int 48: 777-794, 2024.
16. Xiao W, Wang X, Wang T and Xing J: Overexpression of BMP1 reflects poor prognosis in clear cell renal cell carcinoma. Cancer Gene Ther 27: 330-340, 2020.
17. Sun J, Du Y, Zhang X, Wang Z, Lin Y, Song Q, Wang X, Guo J, Li S, Nan J and Yang J: Discovery and evaluation of Atopaxar hydrobromide, a novel JAK1 and JAK2 inhibitor, selectively induces apoptosis of cancer cells with constitutively activated STAT3. Invest New Drugs 38: 1003-1011, 2020.
18. Dinakar YH, Kumar H, Mudavath SL, Jain R, Ajmeer R and Jain V: Role of STAT3 in the initiation, progression, proliferation and metastasis of breast cancer and strategies to deliver JAK and STAT3 inhibitors. Life Sci 309: 120996, 2022.
19. Groner B and von Manstein V: Jak Stat signaling and cancer: Opportunities, benefits and side effects of targeted inhibition. Mol Cell Endocrinol 451: 1-14, 2017.
20. Wang C, Wang Y, Hong T, Cheng B, Gan S, Chen L, Zhang J, Zuo L, Li J and Cui X: Blocking the autocrine regulatory loop of Gankyrin/STAT3/CCL24/CCR3 impairs the progression and pazopanib resistance of clear cell renal cell carcinoma. Cell Death Dis 11: 117, 2020.
21. Song J, Xu S, Zhang ZH, Chen YH, Gao L, Xie DD, Sun GP, Yu DX and Xu DX: The correlation between low vitamin D status and renal interleukin-6/STAT3 hyper-activation in patients with clear cell renal cell carcinoma. Steroids 150: 108445, 2019.
22. Arévalo J, Campoy I, Durán M, Nemours S, Areny A, Vall-Palomar M, Martínez C, Cantero-Recasens G and Meseguer A: STAT3 phosphorylation at serine 727 activates specific genetic programs and promotes clear cell renal cell carcinoma (ccRCC) aggressiveness. Sci Rep 13: 19552, 2023.

23. Ganguly K, Rauth S, Marimuthu S, Kumar S and Batra SK: Unraveling mucin domains in cancer and metastasis: when protectors become predators. Cancer Metastasis Rev 39: 647-659, 2020.
24. Jiang Y, Liu Z, Hu Y, Gao T, Wen T and An G: Correlation of Tn antigen expression with mucins in Chinese patients with colorectal cancer. Int J Clin Exp Pathol 11: 1562-1568, 2018.
25. Miura K, Kinouchi M, Ishida K, Fujibuchi W, Naitoh T, Ogawa H, Ando T, Yazaki N, Watanabe K, Haneda S, *et al*: 5-fu metabolism in cancer and orally-administrable 5-fu drugs. Cancers (Basel) 2: 1717-1730, 2010.
26. Korbut E, Janmaat VT, Wierdak M, Hankus J, Wójcik D, Surmiak M, Magierowska K, Brzozowski T, Peppelenbosch MP and Magierowski M: Molecular profile of barrett's esophagus and gastroesophageal reflux disease in the development of translational physiological and pharmacological studies. Int J Mol Sci 21: 6436, 2020.
27. Su W, Feng B, Hu L, Guo X and Yu M: MUC3A promotes the progression of colorectal cancer through the PI3K/Akt/mTOR pathway. BMC Cancer 22: 602, 2022.
28. Sun Y, Sun X, You C, Ma S, Luo Y, Peng S, Tang F, Tian X, Wang F, Huang Z, *et al*: MUC3A promotes non-small cell lung cancer progression via activating the NFkappaB pathway and attenuates radiosensitivity. Int J Biol Sci 17: 2523-2536, 2021.
29. Luo Y, Ma S, Sun Y, Peng S, Zeng Z, Han L, Li S, Sun W, Xu J, Tian X, *et al*: MUC3A induces PD-L1 and reduces tyrosine kinase inhibitors effects in EGFR-mutant non-small cell lung cancer. Int J Biol Sci 17: 1671-1681, 2021.
30. Liu S, Zhang RF, You Y, You W, Ruan GC, Liu YP, Zhang SY, Li Y, Feng YL, Yan XM, *et al*: The genomic landscape of Cronkhite-Canada syndrome: Possible clues for pathogenesis. J Dig Dis 23: 288-294, 2022.
31. Hammoudeh SM, Hammoudeh AM, Bhamidimarri PM, Al Safar H, Mahboub B, Künstner A, Busch H, Halwani R, Hamid Q, Rahmani M and Hamoudi R: Systems immunology analysis reveals the contribution of pulmonary and extrapulmonary tissues to the immunopathogenesis of severe COVID-19 patients. Front Immunol 12: 595150, 2021.
32. Chen M, Wei X, Shi X, Lu L, Zhang G, Huang Y and Hou J: LncRNA HIF1A-AS2 accelerates malignant phenotypes of renal carcinoma by modulating miR-30a-5p/SOX4 axis as a ceRNA. Cancer Biol Med 18: 587-603, 2021.
33. Zeng K, Song G, Chen B, Gao X, Liu C, Miao J, Ruan Y, Luan Y, Chen X, Liu J, *et al*: Comprehensive analysis to identify the RP11-478C19.2/E2F7 axis as a novel biomarker for treatment decisions in clear cell renal cell carcinoma. Transl Oncol 25: 101525, 2022.
34. Ye S, Li S, Qin L, Zheng W, Liu B, Li X, Ren Z, Zhao H, Hu X, Ye N and Li G: GBP2 promotes clear cell renal cell carcinoma progression through immune infiltration and regulation of PD-L1 expression via STAT1 signaling. Oncol Rep 49: 49, 2023.
35. Xie Z, Feng C, Hong Y, Chen L, Li M and Deng W: Identification of key genes CCL5, PLG, LOX and C3 in clear cell renal cell carcinoma through integrated bioinformatics analysis. Front Mol Biosci 12: 1587196, 2025.
36. Luo Q, Wang Q, Shi J, Lv Q, Dong Z, Li W, Xia Y, Liu J and Yang H: PUMA reduces FASN ubiquitination to promote lipid accumulation and tumor progression in human clear cell renal cell carcinoma. Cell Death Dis 16: 460, 2025.
37. Miao D, Shi J, Xiong Z, Xiao W, Meng X, Lv Q, Xie K, Yang H and Zhang X: As a prognostic biomarker of clear cell renal cell carcinoma RUFY4 predicts immunotherapy responsiveness in a PDL1-related manner. Cancer Cell Int 22: 66, 2022.
38. Liang CC, Park AY and Guan JL: In vitro scratch assay: A convenient and inexpensive method for analysis of cell migration in vitro. Nat Protoc 2: 329-333, 2007.
39. Zheng M, Zhang S, Zhou J, Lin M and Liao Y: ACAT1 suppresses clear cell renal cell carcinoma progression by AMPK mediated fatty acid metabolism. Transl Oncol 47: 102043, 2024.
40. Wang X, Shi A, Liu J, Kong W, Huang Y, Xue W, Yang F and Huang J: CDCA5-EEF1A1 interaction promotes progression of clear cell renal cell carcinoma by regulating mTOR signaling. Cancer Cell Int 24: 147, 2024.
41. Yun Y, Ji X, Wu T, Liu Y, Li Z, Sun Z, Zhou P, Yang L and Yu W: APOC2 promotes clear cell renal cell carcinoma progression via activation of the JAK-STAT signaling pathway. Curr Issues Mol Biol 47: 936, 2025.
42. Shabib S, Rahnama A, Sakhtemanpour Bolouki S, Hosseini SA and Satarzadeh M: JAK/STAT is a main signaling pathway in renal carcinoma: A systematic review of therapeutic potential. J Inflamm Dis 29: e160171, 2025.